SF2A 2011
G. Alecian, K. Belkacem, R. Samadi and D. Valls-Gabaud (eds)

MAPPING THE DUST PROPERTIES OF NEARBY GALAXIES WITH HERSCHEL AND LABOCA

M. Galametz[1], M. Albrecht[2], R. Kennicutt[1], F. Bertoldi[2], F. Walter[3], A. Weiss[4], D. Dale[5], B. Draine[6], G. Aniano[6], C. Engelbracht[7], J. Hinz[7] and H. Roussel[8]

Abstract. We combine Spitzer, Herschel and LABOCA observations from 24 to 870 μm for 11 galaxies of the KINGFISH Herschel Key programme dedicated to the observations of 61 nearby galaxies of various metallicities and levels of star formation activity. We perform a global two-temperature fitting of the Spectral Energy Distributions of the galaxies to study the cold dust properties and probe the variations in the emissivity index of grains inferred by the use of submm data. Using the resolution of Spitzer and Herschel observations, we also produce dust temperature maps of the galaxies and perform a local study of the variations of cold dust properties within the galaxies. We finally build extrapolated maps at 870 μm and compare them with our LABOCA observations. Some of our galaxies exhibit an excess at 870 μm compared to fluxes inferred from the modeling. This excess decreases (and even disappears in some cases) when a lower emissivity index is used, for instance β=1.5 in lieu of the standard value of 2 commonly used in current SED models. The cause for such excess still has to be investigated.

Keywords: ISM, dust, submillimeter, Herschel, LABOCA, SED model

1 Introduction

An exhaustive inventory of the dust temperature distribution and heating processes is essential to understand the physics of the Interstellar Medium (ISM). Numerous studies have pointed out the necessity of both far-infrared (FIR) and submillimeter (submm) observations to constrain the thermal dust emission of galaxies and probe the dust grain properties such as temperature, emissivity or mass (Gordon et al. 2010, among others). *Herschel* is currently mapping nearby galaxies in the 70 to 500 μm wavelength range. Early science results led to the detection of colder dust (T<20K) than previously assumed in nearby galaxies. Those studies investigated the cold dust temperature dependance on morphological type and bars (Engelbracht et al. 2010), radius (Pohlen et al. 2010), star formation or global starlight (Bendo et al. 2011; Galametz et al. 2010). Submm observations of low-metallicity galaxies have also suggested that cold dust properties could differ from standard ones and led to the detection of an excess (Dumke et al. 2004; Galliano et al. 2003, 2005; Bendo et al. 2006; Marleau et al. 2006; Galametz et al. 2009; O'Halloran et al. 2010; Bot et al. 2010). In the present work, we combine *Herschel* observations of 11 nearby galaxies obtained as part of the KINGFISH programme (Key Insights on Nearby Galaxies: A Far-Infrared Survey with Herschel, PI: R. Kennicutt) with LABOCA maps at 870 μm to probe the spatially-resolved cold dust properties and investigate potential submm excess emission in our targets.

[1] Institute of Astronomy, University of Cambridge, Madingley Road, Cambridge CB3 0HA, UK
[2] Argelander-Institut für Astronomie, Abteilung Radioastronomie, Auf dem Hügel, D-53121 Bonn, Germany
[3] Max-Planck-Institut für Astronomie, Königstuhl 17, D-69117 Heidelberg, Germany
[4] Max-Planck-Institut für Radioastronomie, Auf dem Hügel 69, D-53121 Bonn, Germany
[5] Department of Physics & Astronomy, University of Wyoming, Laramie, WY 82071, USA
[6] Department of Astrophysical Sciences, Princeton University, Princeton, NJ 08544, USA
[7] Steward Observatory, University of Arizona, Tucson, AZ 85721, USA
[8] Institut d'Astrophysique de Paris, F-75014 Paris, France

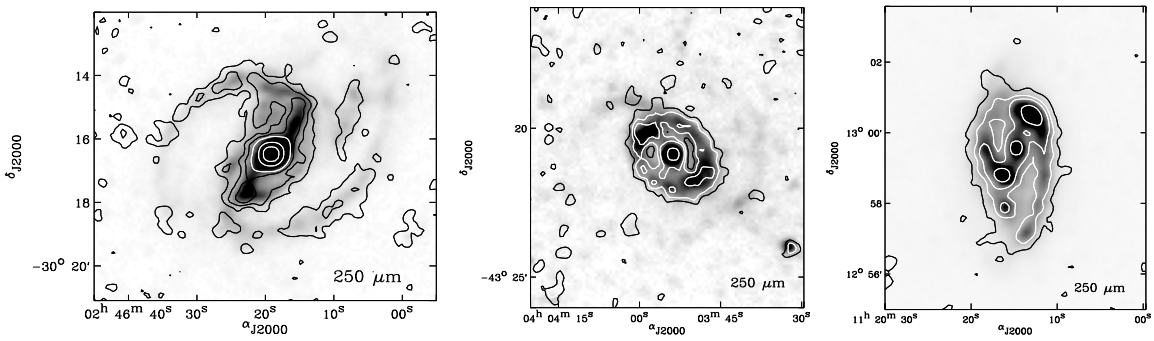

Fig. 1. KINGFISH SPIRE 250 μm observations with 870 μm contours overlaid. **Left:** NGC 1097. Contours indicate flux densities of 4, 10, 17, 30, 100 and 200 mJy.beam^{-1}, **Middle:** NGC 1512. Contours indicate flux densities of 3.5, 6.5, 10 and 25 mJy beam^{-1}. **Right:** NGC 3627. Contours indicate flux densities of 10, 30, 50 and 100 mJy beam^{-1}.

2 Herschel and LABOCA observations

The *Herschel* PACS and SPIRE observations have been obtained as part of the KINGFISH programme (see Kennicutt et al. 2011, for a description of the survey). PACS observes at 70, 100 and 160 μm with FWHMs of 5.2", 7.7" and 12" respectively (Poglitsch et al. 2010). The Scanamorphos technique was used to process the data from Level 1 (Roussel et al. 2011 in prep). The PACS calibration uncertainties are $\sim$10 % at 70 and 100 μm and $\sim$20 % at 160 μm. SPIRE produces maps at 250, 350 and 500 μm, with FWHMs of 18", 25" and 36" respectively (Griffin et al. 2010). Calibration uncertainties are estimated to be $\sim$7% for the three wave bands. Complementary data with LABOCA at 870 μm were also obtained for the same sample. A complete description of the LABOCA data reduction can be found in Albrecht et al. (in prep). The full width half maximum (FWHM) of the point spread function (PSF) at 870 μm is $\sim$19".2. The resolution of LABOCA is similar to that of SPIRE 250 μm. SPIRE 250 μm maps with LABOCA contours overlaid are shown in Fig. 1.

3 Global dust properties

To study the global dust temperatures of our sample, we perform a two-temperature (warm and cold) modeling with a combination of modified blackbodies. We add *Spitzer* and IRAS data to sample the dust thermal emission of our galaxies from 24 to 870 μm. The notation T_c will refer to the temperature of cold dust hereafter. The emissivity index of the warm dust (β_w) is fixed to a standard emissivity index of 2 (Li & Draine 2001) while that of the cold dust (β_c) is free. Figure 2 *left* shows the global SED of NGC 3627. The bottom panel indicates the residuals from the fit. For NGC 1097, NGC 1512, NGC 3351 or NGC 3621, the warm component contributes to more than 50% of the 70 μm flux, justifying the use of a warm component in the fitting. We observe strong variations of the cold dust emissivity within our sample, with β_c varying between 0.96 to 2.12 (consistent, within the error bars, with the expected range for emissivities). The LABOCA 870 μm flux strongly influences the parameters derived in some cases like NGC 1512 (steeper emissivity required). We note that the 500 μm flux density is systematically underestimated by the model when the LABOCA flux is used in the modeling. This excess is lower than 20 % for most of the galaxies but reaches 40 % for NGC 1512. We find that the derived T_c are higher when β_c is free compared to values derived if β_c is fixed to a standard value of 2. In that last case, the use of LABOCA data only weakly influences the T_c estimate (less than 4%).

Instrumental uncertainties can lead to an anti-correlation between T and β (Shetty et al. 2009). In order to study this dependence and quantify the errors bars of our results, we generate for each galaxy 2000 sets of modified constraints randomly varying within error bars. Correlations between SPIRE calibration errors are taken into account when generating the new datasets. We apply our two-temperature fit to the 2000 modified sets. Figure 2 *right* shows the parameter distribution of the 2000 runs in a T_c - β_c parameter space for NGC 3627. The green crosses indicate the 2000 (T_c, β_c) combinations derived when the correlation between SPIRE calibration uncertainties is taken into account and the black crosses the 2000 combinations where SPIRE fluxes are modified independently. We overlay the median temperature and emissivity index in red. Taking into account the correlations between SPIRE calibration uncertainties clearly shrinks the ranges of values reached by T_c and β_c but does not influence the median values derived (less than 2% difference).

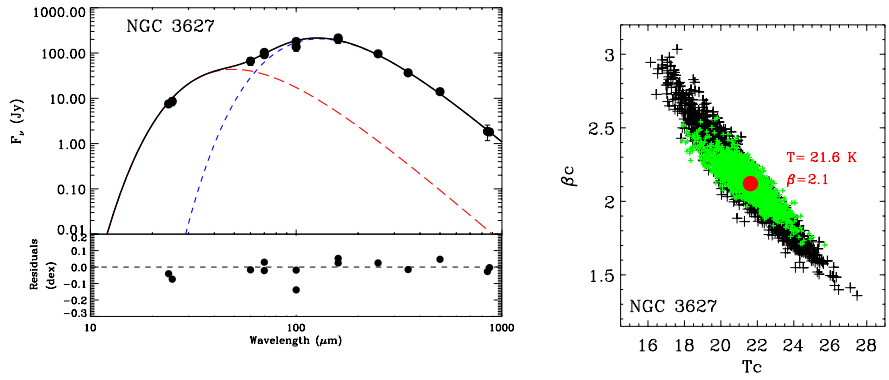

Fig. 2. Left: Two-temperature fits for NGC 3627 (β_w=2, β_c free). Data are overlaid with black circles. The bottom panel indicates the residuals from the fit. **Right:** (T_c, β_c) combinations derived from 2000 randomly modified datasets for NGC 3627. Median values are overlaid in red. See text for details on definitions and colors.

4 Resolved temperature maps

We use the same two-temperature modeling technique to derive temperature maps. MIPS, PACS and SPIRE maps are convolved to the SPIRE 500 μm resolution and projected to a common sample grid with a pixel size of 18". We first use a fixed β_c (=2) to obtain a robust determination of the cold dust temperature distribution. LABOCA data are not used in the fitting but combined with the procedure results to derive excess maps at 870 μm (see the next section). Figure 3 *left* shows the temperature map of NGC 3627. SPIRE 250 μm contours are overlaid to enable a comparison of the temperature distribution with submm emission. We observe a smooth variation of the cold dust temperature distribution within our galaxies, with temperature maxima towards the center and towards star forming regions, and temperatures decreasing in the outer parts of galaxies. The choice of β_c=2 influences the temperatures derived. The temperature range is globally scaled to higher values if $\beta_c <$ 2 or lower values if $\beta_c > 2$. If we let T_c and β_c vary, the temperature distributions derived from the modeling are more homogenous than those obtained with a fixed β_c, with a disappearance of the galaxy structure in extended objects. The temperature distribution seems also more erratic for low-surface brightnesses. This effect was pointed out by Planck Collaboration et al. (2011b) in the LMC and by Foyle et al. 2011 (submitted) in M83.

These discrepancies between temperature maps of course questions the physical sense of letting both temperature and emissivity vary at the same time, knowing the possible correlation between those parameters. Figure 3 shows the T-β diagram gathering pixels with 500 μm 3-σ detection for our sample. Galaxies are color-coded. The distribution of pixels in the T-β plane significantly differs from galaxy to galaxy, with a wide range of emissivity values for galaxies such as NGC 628, NGC 1097, NGC 3621 or NGC 7793, or more homogeneous values for NGC 1512, NGC 3351 or NGC 3627. An anti-correlation is clearly observed between temperature and emissivity, with higher emissivity values in colder ISM elements. The trend does not disappear if we restrict ourselves to the brightest pixels (so good confidence in the flux densities). It thus seems unlikely that this anti-correlation is only linked with Eddington bias (i.e. uncertainties on measurements) even if this assumption is difficult to assess. Moreover, a 18" × 18" pixel corresponds to a large ISM element for the galaxies of our sample - 18" corresponds to ∼0.8 kpc at the distance of NGC 3627 - and thus to a large mixture of dust temperatures. The anti-correlation could then be artificially created by the addition of several dust temperatures, with a flattening of the slope when cold dust is present along the line of sight. Studies on resolved structures in the Milky Way (e.g. Paradis et al. 2009; Planck Collaboration et al. 2011a) or in closest galaxies like the Magellanic Clouds are crucial to better disentangle these explanations.

5 Investigations on a submm excess

Previous submm observations have led to the detection of an excess compared to extrapolations from *Spitzer*-based fits, especially in low-metallicity galaxies. This excess is poorly understood and a spatially-resolved study is necessary to understand its origin and link it with the properties of the environment. One of the major

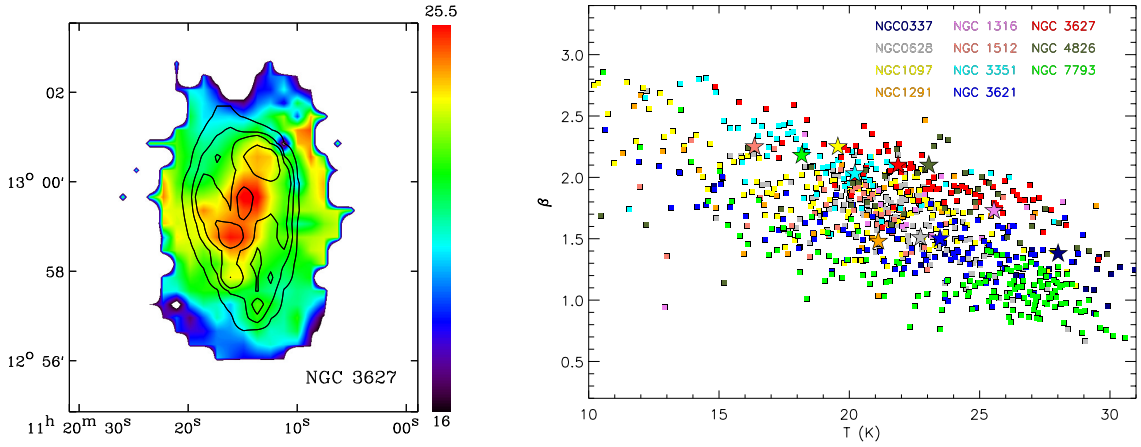

Fig. 3. Left: Temperature maps in Kelvin derived with $\beta_c = 2$. SPIRE 250 μm contours are overlaid. **Right:** Temperature dependence of the spectral index in our sample. Global estimates are shown with stars. Squares are pixel-by-pixel values (pixel size: 18") averaged 3-by-3 for clarity.

interests of our study is that submm excess was never detected in a normal spiral galaxy before. For that matter, none of our galaxies show an excess at 870 μm when studied globally. The resolutions of *Herschel* and LABOCA maps enable us for the first time to study if an excess is detected at local scales. We use the previous modeling technique (based on data up to 500 μm) to extrapolate a 870 μm map. β_c is fixed to 2, 1.5 or used as a free parameter. We convolve and regrid our LABOCA maps to match our 18" pixel grid and calculate the LABOCA excess compared to the extrapolated maps at 870 μm. A pixel-by-pixel SED modeling of the whole KINGFISH sample using the more complex Draine & Li (2007) dust models is performed in Aniano et al. (in prep). We extrapolate 870 μm maps from their procedure and compare them with our LABOCA data as well.

Figure 4 shows the 870 μm excess maps in absolute scale (LABOCA maps - extrapolated maps) obtained using our two-temperature fits with β_c fixed to 2, 1.5 or free. Some extended galaxies possess a clear 870 μm excess that seems to follow the bright structures of the galaxies (NGC 337, NGC 1097, NGC 1512, NGC 3627, NGC 4826) while others do not present such an excess (e.g. NGC 628). The 870 μm maps extrapolated using $\beta_c = 1.5$ are brighter than those using $\beta_c = 2$ due to the flatter submm slope induced by the modeling technique. The excess derived using $\beta_c = 1.5$ is thus systematically lower than that with $\beta_c = 2$ and disappears in some cases (e.g. NGC 1512, NGC 3621). The excess maps derived using the Draine & Li (2007) formalism are most of the time in between the two models with $\beta_c = 2$ and $\beta_c = 1.5$. It might be explained by the fact that in the wavelength range covered by SPIRE, their SEDs are similar to modified blackbodies with $\beta_c = 2$ but more flexible due to the mixture of temperatures it includes. We remind the reader than those models also incorporate modifications in the amorphous silicate opacity at $\lambda > 250$ μm, in order to better match the average high Galactic latitude dust emission spectrum measured by COBE-FIRAS (Wright et al. 1991; Reach et al. 1995; Finkbeiner et al. 1999) and thus already include a "submm excess" (lower than 12 % at $\lambda > 250$ μm).

We are still investigating the origin of the 870 μm excess. Several sources of line emission can contaminate the 870 μm flux and contribute to the excess, for instance the ^{12}CO(3-2) line whose rest wavelength (867 μm) falls into the LABOCA spectral bandpass. Two galaxies (NGC 1512 and NGC 3621) do not have any CO measurements while half of our sample only possess single-point ^{12}CO(3-2) or ^{12}CO(1-0) measurements toward the center. Four galaxies (NGC 337, NGC 628, NGC 3351 and NGC 3627) have been mapped in ^{12}CO(3-2) and/or in ^{12}CO(2-1) as part of the James Clark Maxwell Telescope Nearby Galaxies Legacy Survey (NGLS; Wilson et al. 2009) and HERA CO Line Extragalactic Survey (HERACLES; Leroy et al. 2009) respectively. Those maps will help us to quantify the contribution of the ^{12}CO(3-2) line to the 870 μm flux directly or using CO line ratios. Secondary sources of contamination are the synchrotron emission from relativistic electrons moving in a uniform magnetic field or thermal bremsstrahlung emission (free-free) from electrons in the hot ionized gas. Those contributions will be estimated using available radio and Hα maps of the galaxies. Only then will we be able to properly quantify the relative excess of our galaxies at 870 μm.

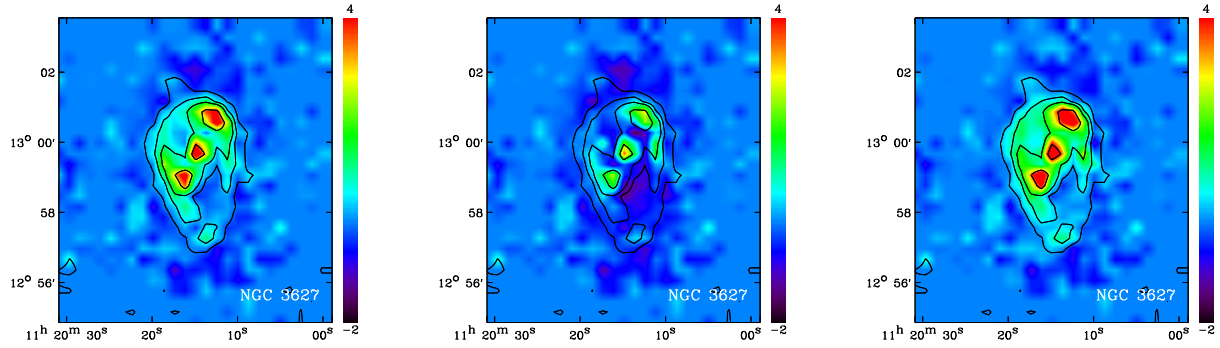

Fig. 4. Excess map at 870 μm of NGC 3627 (in MJy sr^{-1}) derived using our two-modified blackbody procedure with, from left to right, β_c fixed to 2, fixed to 1.5 or free.

References

Bendo, G. J., Boselli, A., Dariush, A., et al. 2011, arXiv:1109.0237
Bendo, G. J., Dale, D. A., Draine, B. T., et al. 2006, ApJ, 652, 283
Bot, C., Rubio, M., Boulanger, F., et al. 2010, A&A, 524, A52+
Draine, B. T. & Li, A. 2007, ApJ, 657, 810
Dumke, M., Krause, M., & Wielebinski, R. 2004, A&A, 414, 475
Engelbracht, C. W., Hunt, L. K., Skibba, R. A., et al. 2010, A&A, 518, L56+
Finkbeiner, D. P., Davis, M., & Schlegel, D. J. 1999, ApJ, 524, 867
Galametz, M., Madden, S., Galliano, F., et al. 2009, A&A, 508, 645
Galametz, M., Madden, S. C., Galliano, F., et al. 2010, A&A, 518, L55+
Galliano, F., Madden, S. C., Jones, A. P., Wilson, C. D., & Bernard, J.-P. 2005, A&A, 434, 867
Galliano, F., Madden, S. C., Jones, A. P., et al. 2003, A&A, 407, 159
Gordon, K. D., Galliano, F., Hony, S., et al. 2010, A&A, 518, L89+
Griffin, M. J., Abergel, A., Abreu, A., et al. 2010, A&A, 518, L3+
Kennicutt, Jr., R. C. et al. 2011, submitted to PASP
Leroy, A. K., Walter, F., Bigiel, F., et al. 2009, AJ, 137, 4670
Li, A. & Draine, B. T. 2001, ApJ, 554, 778
Marleau, F. R., Noriega-Crespo, A., Misselt, K. A., et al. 2006, ApJ, 646, 929
O'Halloran, B., Galametz, M., Madden, S. C., et al. 2010, A&A, 518, L58+
Paradis, D., Bernard, J.-P., & Mény, C. 2009, A&A, 506, 745
Planck Collaboration, Abergel, A., Ade, P. A. R., et al. 2011a, arXiv:1101.2037
Planck Collaboration, Ade, P. A. R., Aghanim, N., et al. 2011b, arXiv:1101.2046
Poglitsch, A., Waelkens, C., Geis, N., et al. 2010, A&A, 518, L2+
Pohlen, M., Cortese, L., Smith, M. W. L., et al. 2010, A&A, 518, L72+
Reach, W. T., Dwek, E., Fixsen, D. J., et al. 1995, ApJ, 451, 188
Shetty, R., Kauffmann, J., Schnee, S., Goodman, A. A., & Ercolano, B. 2009, ApJ, 696, 2234
Wilson, C. D., Warren, B. E., Israel, F. P., et al. 2009, ApJ, 693, 1736
Wright, E. L., Mather, J. C., Bennett, C. L., et al. 1991, ApJ, 381, 200